Modeling sediment movement and channel response to rainfall variability after a major earthquake

Jun Xie, Ming Wang, Kai Liu, Tom J. Coulthard

Abstract

The 2008 Wenchuan Ms 8.0 earthquake caused severe destruction in the mountainous areas of Sichuan Province, China. Landslips and mass movements led to substantial amounts of loose sediment accumulating in valleys that subsequently led to widespread riverbed aggradation. In addition to erosion and deposition hazards, this aggradation produced rivers in earthquake affected areas that were more susceptible to flash floods under extreme rainfall events. However, fluvial processes and sediment movement after a major earthquake, as well as the re-working of sediments in future events, are not well studied. In this paper, we investigate the response of sediment and river channel evolution due to different rainfall scenarios after the Wenchuan earthquake by using the CAESAR-Lisflood model. This is the first time this landscape evolution model has been employed to explore material migration processes in a post-earthquake area, and to test its applicability to real landform changes in the studied catchment. The CAESAR-Lisflood model is well suited to simulate sediment movement, particularly the fluvial processes driven by severe rainfall after an earthquake. We calibrated the model parameters to the 2013 extreme rainfall event using high-resolution satellite images. Under rainfall scenarios of different intensity and frequency over a 10-yr period, landform evolution and sediment migration in the post-earthquake area were simulated. The results showed that the sediment yield could

be significantly increased under enhanced and intensified rainfall scenarios compared to a normal rainfall scenario. These findings are of importance for the planning of post-earthquake rehabilitation and regional sustainable development, which considers risk prevention and mitigation.

Keywords: Fluvial processes, CAESAR-Lisflood, Rainfall, Earthquake

1. Introduction

The Wenchuan Ms 8.0 (surface-wave magnitude) earthquake occurred in the vast mountainous areas of the Sichuan Province of China and caused severe destruction. Thousands of landslides and rock falls were triggered by the earthquake and associated aftershocks, with 257 landslide lakes formed in the earthquake-stricken area (Cui et al., 2009). These secondary hazards induced by the major earthquake have greatly changed the land use and land cover in the area, especially the significant vegetation loss and degradation that leads to increased soil erosion. According to previous studies, the amount of all types of soil erosion (including the landslides, slumps, slips, fluvial and diffusive erosion) caused by the Wenchuan earthquake is over 5500 million m^3 (Chen et al., 2009), which is equivalent to one year’s worth of soil erosion for all of China during normal years.

Research has indicated that the areas stricken by the Wenchuan earthquake would experience a prolonged influence in the mountainous environment (Xu, 2009; Tang, 2010; Tang et al., 2011; Huang and Li, 2014). For example, the accumulated deposition of loose materials in upper gullies can become debris flows during severe rainfalls, and the elevated riverbeds caused by the movement and aggradation of enormous volumes of loose materials leads to a decrease of discharge capacity and increases the susceptibility to flash floods. Over the next decade, the post-earthquake reconstruction will face great challenges due to various mountain disasters such as debris flows, landslides and flash floods (Xu, 2009). Through the study of post-earthquake, rainfall-induced channel movement and erosion response (Chen et al., 2014), the energy involved in the transportation of deposits is expected to be considerable. Loose materials will continue to accumulate in valleys and on hillslopes, and their movements, which are induced by natural and man-made disturbances (i.e., severe rainfall or road construction), will persist for decades (Wang et al., 2015). Secondary disasters such as debris flows, new and expanded landslides triggered by severe rainfall after major earthquakes have a direct link to regional land surface erosion (Chang et al., 2006; Chen et al., 2006; Korup et al., 2010). Landslides combined with subsequent, severe rainfall are the main sources of deposition and transportation of mountainous material, which becomes one of the key factors in the channel evolution process in mountainous areas after a major earthquake. The movement of fragmentary materials in valleys and on slopes increases the deposition and aggradation of river channels (Qi et al., 2012).

Although there have been several studies exploring the impact of landslides and debris flows on channel evolution (e.g., Korup, 2009), few studies have looked at the evolution of the changes in disaster affected areas and quantitatively assessed the dynamics of changing risks. Geological hazards that occur in mountainous environments after a major earthquake can be a long-term threat. Key tasks for studying the long-term impact of subsequent disasters in earthquake-stricken regions are to understand channel change mechanisms after a major earthquake and to simulate the associated dynamic processes (Chen et al., 2014). Furthermore, the aggradation of riverbeds can make earthquake impacted areas extremely susceptible to flash floods, thereby creating further risks to newly rebuilt houses near the river (Yang et al., 2015).

In this study, we attempt to answer the following three research questions. (1) How reliable is the landscape evolution model (CAESAR-Lisflood) in simulating material migration processes in a post-earthquake area? (2) How do sediment production and sediment yields respond to rainfall variability? (3) How does the geomorphology, especially the river channel, evolve under future rainfall scenarios with more frequent extremes? Basin wide processes of erosion and deposition under high rainfall, in an earthquake affected region is investigated using the CAESAR-Lisflood (CL) model (Coulthard and Wiel, 2013). We used CL in the Hongxi River in Sichuan, China, to simulate the channel changes that occurred in 2013 (five years after the Wenchuan earthquake), following landslides and debris flows due severe rainfall events. We compared the modeling results with observed channel changes from both field investigation and high-resolution satellite images. The sediment yield and landform evolution in the study area were then assessed using hypothetical future rainfall scenarios.

2. Study area

The Hongxi River catchment, an upstream tributary of the Fu River, is located in Pingwu County of the Sichuan Province (Fig. 1). The drainage area of this catchment is approximately 179 km^2 and the overall length is 31 km. The average discharge is 2.0 m^3/s

and the average annual precipitation in this catchment is ~700 mm. The topography of the catchment is rugged with an elevation ranging between 679 and 3036 m. Because of the high and steep terrain, this area was one of the most severely affected locations during the Wenchuan earthquake with a Modified Mercalli Intensity (MMI) scale of IX and X (Wang et al., 2014). The MMI scale is a seismic scale used for measuring the intensity (or the effects) of an earthquake, and it quantifies the seismic intensity from I to XII, from ‘not felt’ to ‘total destruction’. The Ma An Shi landslide and Wen Jia Ba landslide were among the largest landslides that occurred during the earthquake. The lake created along the Hongxi River by the Wen Jia Ba landslide was among the largest three created (Cui et al., 2009). Ten years after the Wenchuan earthquake, the Hongxi River basin still experienced frequent, subsequent landslides and debris flows triggered by severe rainfall. As shown in Fig. 1, the areas in red indicate the locations of landslides and debris flows that occurred following intense rainfall in 2013. Figure 2 shows the typical sites of new landslides, debris flows, erosion and deposition that occurred in the study area.

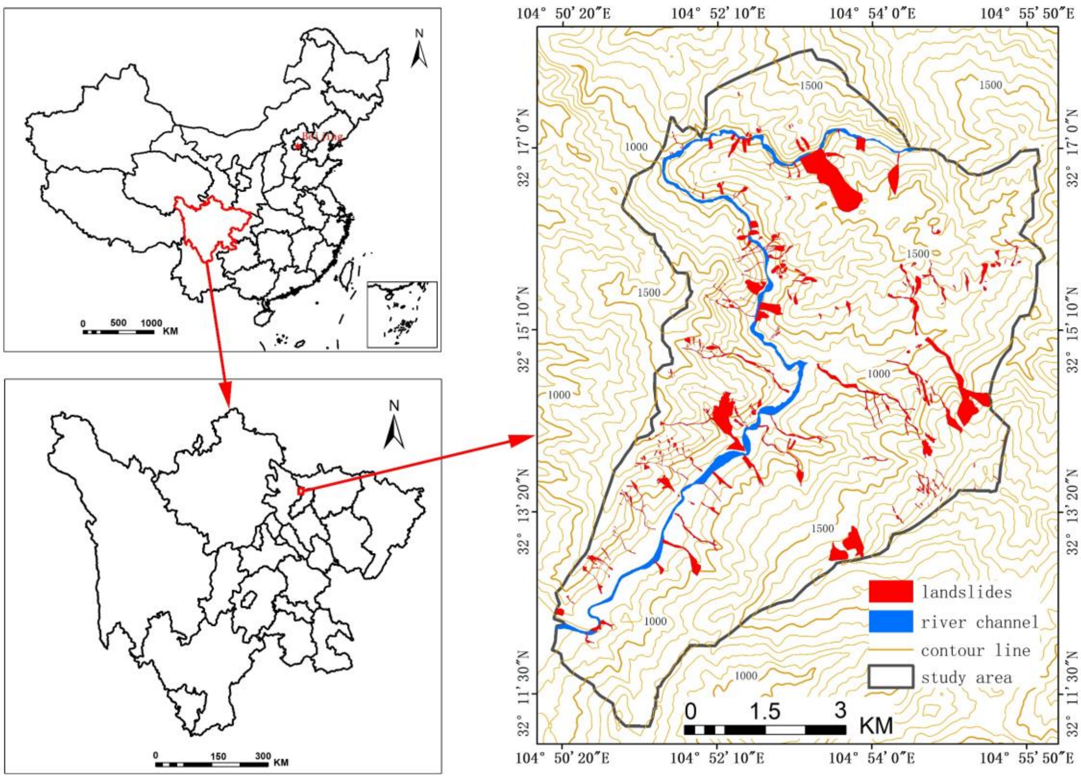

Fig. 1. Geographic location of the study area.

Fig. 2. Typical sites of geo-hazards in the study area (a) new landslide, (b) erosion, (c) deposition, (d) debris flow and damaged check dam, (e) damaged village by flood and debris flow.

The changes in the river channel of different years, and landslides and debris flows after the 2013 flooding in the study area were manually extracted from high-resolution satellite images. Five 1-A level high-resolution satellite images before and after the 2008 earthquake were collected and listed in Table1. We used an IKONOS image in November 2002, a WorldView image in April 2012, and a GF-2 image in August 2015 to extract and identify the channel changes in 2002, 2012 and 2015. We used a SPOT-6 image in October

2012 and an IKONOS image in December 2013 to compare the changes of typical sites impacted by the 2013 flooding.

Table 1 Inventory of satellite images used.

Time	Sensor	Panchromatic Resolution (m)	Multispectral Resolution (m)	Extraction
November 2002	IKONOS	1	4	River channel
April 2012	WorldView-1	0.5	---	River channel
August 2015	GF-2	0.8	2.5	River channel
October 2012	SPOT-6	1.5	5	Typical sites before 2013 flooding
December 2013	IKONOS	1	4	Typical sites after 2013 flooding and landslides/debris flow of study area

Continuous monitoring in this study area indicates that the persistent downward movement of landslide debris has rapidly aggraded riverbeds of the Hongxi River over the past eight years. Two obvious changes occurred in the river channel of the Hongxi Basin after the Wenchuan earthquake in 2008 and following the extreme rainfall in 2013. Through the visual interpretation of three high-resolution satellite images (IKONOS of 2002, WORLDVIEW of 2012 and GF-2 of 2015 as listed in Table 1), we extracted the boundary of the river channel in 2002, 2012 and 2015 (Fig. 3) to identify the channel changes. Compared with the pre-earthquake channel, rapid increases in riverbed width was clearly observed. The channel width increased up to 146 m between 2012 and 2002, up to 160 m between 2015 and 2002, and up to 123 m between 2015 and 2013. In most areas, the channel width almost doubled on average after 2008. From 2012 to 2015, channel width continued to increase, particularly in the downstream segments due to extreme rainfall and flash flooding. Figure 4 shows an example of the channel changes in different years at the same location, as interpreted from the satellite images.

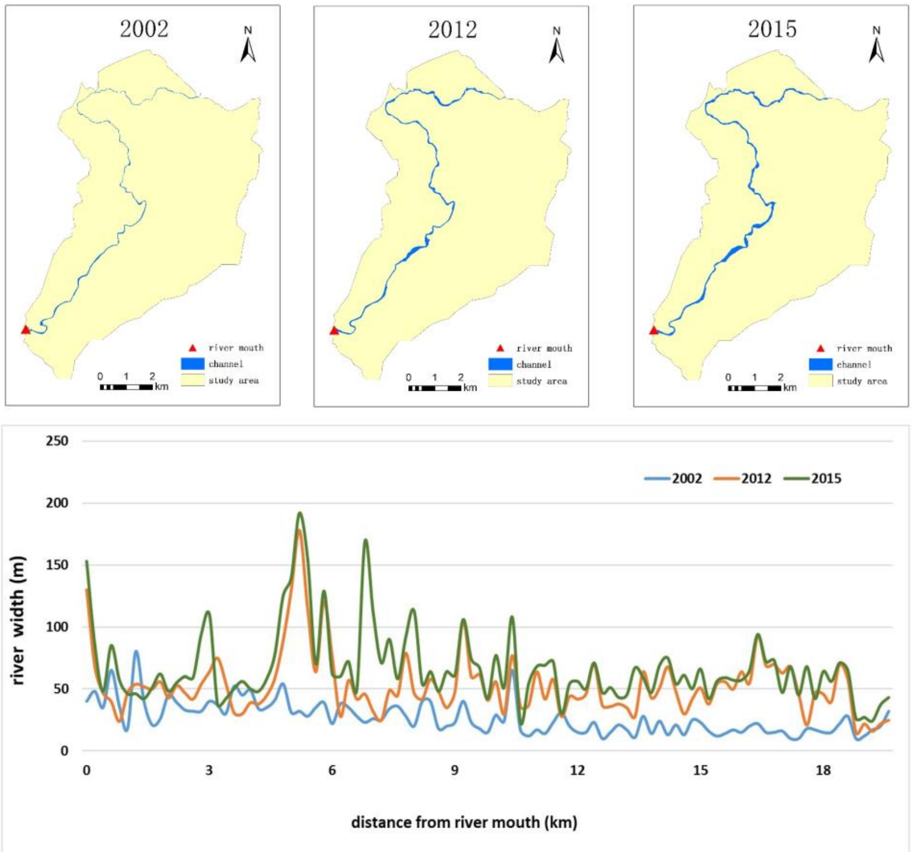

Fig. 3. Study area and channel changes in 2002, 2012, 2015.

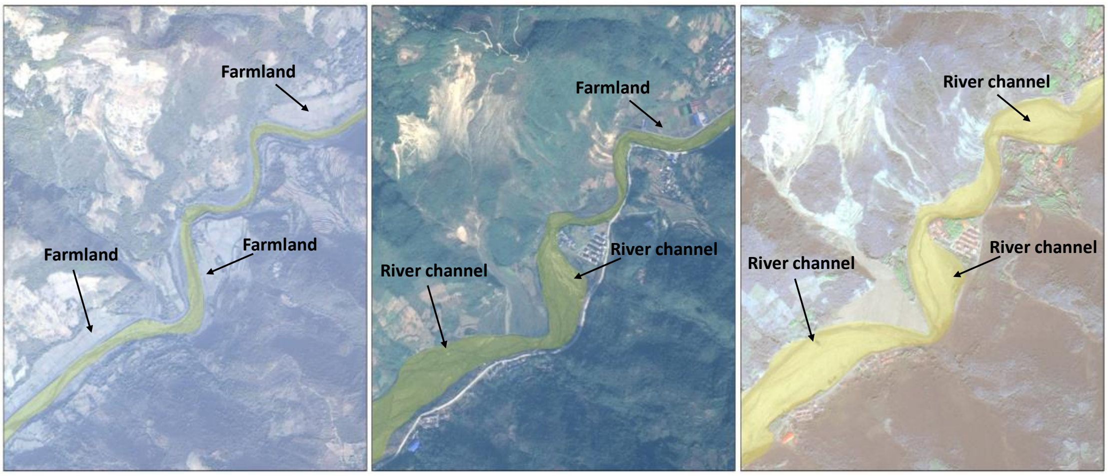

(a) Year of 2002, before the earthquake

(b) Year of 2012, after the earthquake

(c) Year of 2013, after the flooding

Fig. 4. Example of river channel (light yellow) changes in different years.

3. Methods

Since the late 1970s, computer-based numerical models have been developed to simulate the interaction of fluvial process and landscape evolution over long time scales (Hancock et al., 2015). Landscape evolution models (LEMs) consider surface runoff and channel flow as the principal components for sediment processes. Recently, CAESAR-Lisflood was developed, which has a wide range of advantages and can accurately simulate channel evolution under different scenarios (Coulthard et al., 2013). The CAESAR-Lisflood model was initially developed to examine the natural catchment hydrology and geomorphology, and it has become a tool to simulate geomorphic behaviors such as erosional and depositional changes in river catchments over a range of temporal and spatial scales (Coulthard et al., 2013). We used CAESAR-Lisflood in this study to simulate channel movement and landscape change response to rainfall variability, as well as to investigate the potential risks of multi-hazards (flooding, erosion and deposition) to post-earthquake reconstruction in the study area.

3.1. CAESAR-Lisflood

CAESAR-Lisflood is a raster-based model that simulates the evolution of landforms that are subject to fluvial and diffusive erosion and mass movement processes. The model integrates the lisflood-FP 2D hydrodynamic model (Bates et al., 2010) with the CAESAR model (Coulthard et al., 2002). In CAESAR-Lisflood, the catchment is divided into a mesh of grid cells, and for each cell the model stores values of elevation, grain-size and hydrological parameters (e.g., discharge, water depth, etc.). During the model run, the values in each cell are updated in relation to the immediate neighbors according to a series of laws. These include hydrological routing, flow routing, erosion and deposition, and slope processes.

3.2. Model input

In this study, the basic parameters of the model include four key inputs: the digital elevation model (DEM) of the catchment, rainfall (mm/hr), grain-size distribution of the sediment and the vegetation conditions.

3.2.1. DEM

The current landforms in the study area are quite different from those observed before the earthquake (Li et al., 2018). A 10 m resolution DEM (2010) of the Hongxi River catchment was obtained through the GlobalDEM product, which is based on InSAR data and high-resolution satellite stereo imagery. The GlobalDEM is an off-the-shelf product featuring high accuracy, high resolution, noiselessness, and low cost, and it has more than 90% of the world's terrestrial coverage. The GlobalDEM has a spatial resolution with a 10 m x 10 m raster and 5 m (absolute) vertical accuracy. This DEM is the most recent one that could represent the post-earthquake surface conditions before the occurrence of extreme rainfalls in 2013. Because the model running time showed an exponential growth with an increase in DEM resolution, the GlobalDEM was resampled at a coarser resolution of 20 m to maintain model stability and achieve a high operating speed for the model.

3.2.2. Rainfall of 2013

In 2013, there were two severe rainfall events in the study area that led to the two main floods that occurred in July and August. For the calibration of CAESAR-Lisflood, we chose the 2013 rainfall as the input data for the model calibration to simulate these 2013 events. We generated an entire year of hourly rainfall data based on the resampled 3-h TRMM (Tropical Rainfall Measuring Mission) product.

3.2.3. Grain-size distribution

Sediment particle size data were obtained based on soil samples collected from 14 representative locations (Fig. 5) in the channel, near the channel, and on the hillslope at an average depth of one meter. We averaged these data to generate the input particle size information. Figure 6 shows the mean, upper and lower bounds of the cumulative probability of the grain size distribution in these samples.

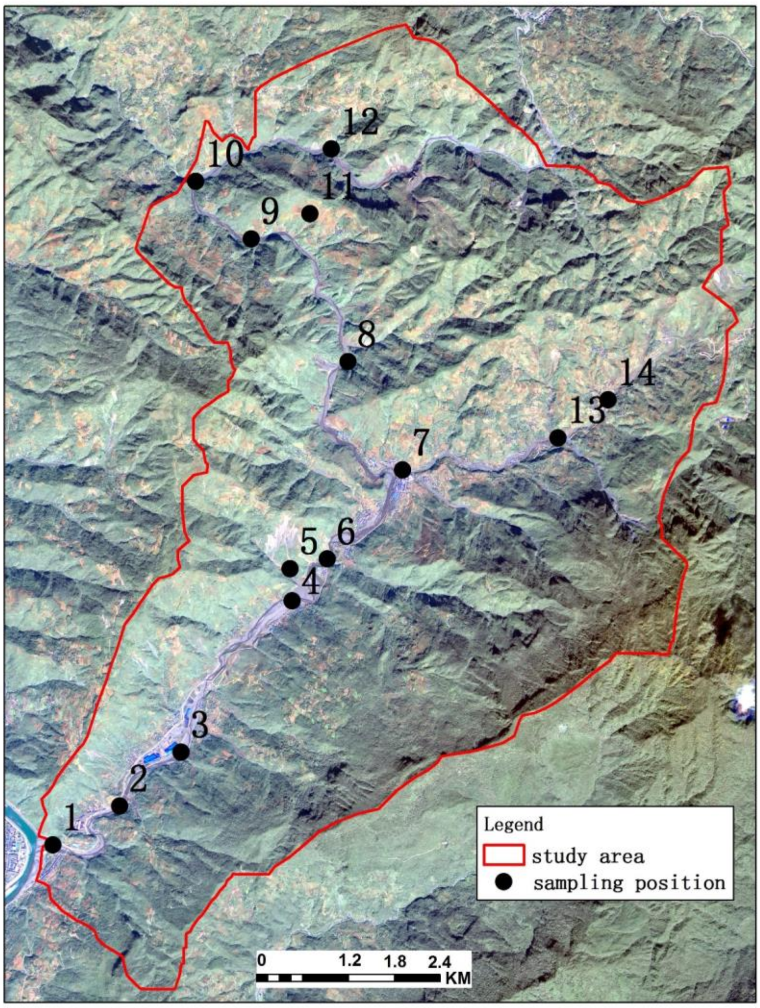

Fig. 5. Spatial distribution of the sampling points in the study area.

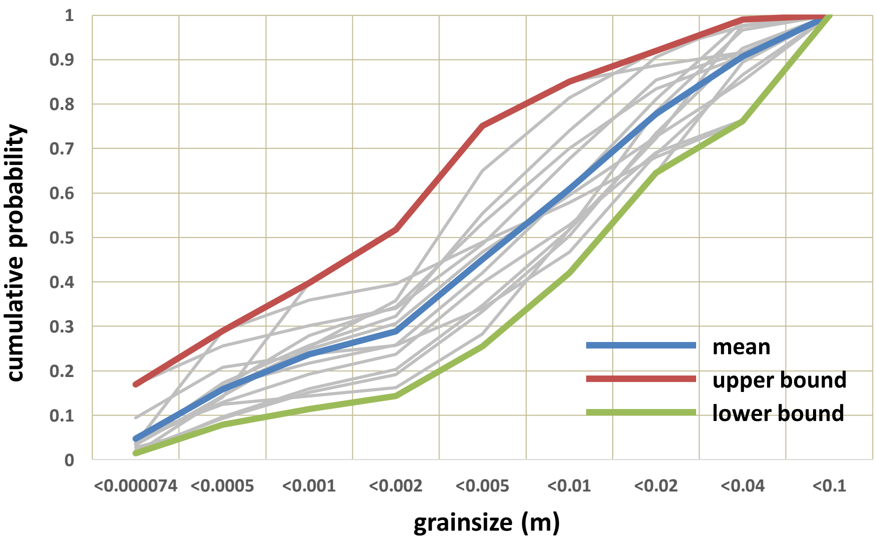

Fig. 6. Cumulative probability of sediment particle size from the 14 sampling points.

3.2.4. Vegetation conditions

In CAESAR-Lisflood, land-use (vegetation) changes can be altered to change the hydrology (m value) of the catchment. For the catchment mode, the m valve is an important parameter because it controls the peak and duration of the hydrograph in response to rainfall and is derived from the m value of TOPMODEL, upon which the CAESAR-Lisflood hydrological model is based (Coulthard et al., 2002). The typical m value ranges from 0.005 (low vegetation) to 0.02 (well forested). The Wenchuan earthquake in 2008 resulted in numerous landslides that disturbed vast areas of vegetation and changed the initial ground conditions prodigiously. Recent additions to CL (Coulthard and Wiel, 2017) enabled spatially variable values of m to be used (e.g., 0.02 for forest, 0.005 for grassland) to represent different land uses to explore long-term basin scale sediment connectivity. In this study, we represented areas of different land use by using high-resolution satellite images and classified the land use into four types, which included forest, farmland, landslide and river channel. We calculated the normalized difference vegetation index (NDVI) of each land use type for 2013 to represent the vegetation conditions in our study area. Then, the m values for forest, farmland, landslide and river channel were set for 0.02, 0.008, 0.003 and 0.002, respectively, through a linear interpolation between 0.005 and 0.02. Table 2 shows the main parameters of the simulation.

Table 2 Model input parameters.

CAESAR-Lisflood parameter	Values	Description of parameter
Grain sizes (m)	0.000074, 0.0005, 0.001, 0.002, 0.005, 0.01, 0.02, 0.04, 0.1	Used for sediment transporting calculation in each active layer (Wiel et al., 2007)
Grain size	0.098, 0.138, 0.052,	Denotes the fractional volume of the grain-size in

proportions	0.162, 0.158, 0.169, 0.13, 0.06, 0.033	each active layer (Wiel et al., 2007)
Sediment transport law	Wilcock and Crowe equations	Works with multiple grain sizes across the sand and gravel range (Coulthard et al., 2007)
Max erode limit (m)	0.02	The maximum amount of material that can be eroded or deposited within a cell at each time step (Coulthard et al., 2013)
Active layer thickness (m)	0.1	The thickness of a single active layer (Wiel et al., 2007)
Lateral edge smoothing passes	0.000001	The variable controls lateral erosion (Coulthard et al., 2013)
Soil creep/diffusion value	0.025	The variable that forms part of the USLE equation (Hancock et al., 2011)
Slope failure threshold	65	Angle threshold in degrees above which landslides happen (Hancock et al., 2011)
Evaporation rate (m/day)	0	Used to calculate the evapotranspiration
Courant number	0.7	The value controls the numerical stability and speed of operation of the flow model (Coulthard et al., 2007)
Manning's n	0.04	The roughness co-efficient used by the flow model (Beven, 1997)

3.2.5. Future rainfall scenarios

For the modeling of future conditions, we generated three rainfall scenarios to explore the sediment migration and geomorphological evolution response to rainfall variability. In this study area, the 2013 rainfall (1458.3 mm) was the most extreme between 1954 and 2016 because it was the wettest season on record. The 2016 rainfall (683 mm) is a normal rainfall year compared to historical record. Therefore, we used the 2013 rainfall as the 'extreme' year and the 2016 rainfall as the reference 'normal' year in the creation of the future rainfall scenarios. The rainfall in the extreme year is almost twice that of the normal year. These two years of rainfall data were used to generate the three different rainfall scenarios used as input into the CAESAR-Lisflood model (Table 3 and Fig. 7). First, ten years of data were created synthetically for the normal rainfall scenario by adding the 2016 rainfall end to end. We used this normal scenario as the basic reference scenario. Second, two years of normal rainfall were combined with one year of extreme rainfall data to generate three years of enhanced rainfall. This three-year period of rainfall was duplicated end-to-end to produce ten-year rainfall scenarios. We consider these datasets enhanced rainfall data, which include a return interval of three years for the 2013 extreme year to represent the trend of more frequent extreme rainfall in the future (enhanced scenario). Third, ten years of intensified rainfall was generated by multiplying the normal rainfall scenarios by 1.5 (intensified scenario). This rainfall scenario explores the channel migration and sediment yield that would occur by strengthening the average rainfall. Since the extreme year has almost twice the rainfall of a normal year, we used a factor of 1.5 to create an intensified rainfall year that was intermediate between a normal and an extreme year. Each year in the intensified scenario has the same amount of rainfall, which is different from the enhanced rainfall in which extreme rainfall occurs every three years. Therefore, the intensified rainfall scenario represents an overall increased rainfall setting in the future, rather than more frequent extreme years.

Table 3 Three hypothetical rainfall scenarios used as modeling input.

Scenarios	**Period (year)**	**Average annual precipitation (mm)**	**Notes**
Normal	10	684	10 years of ‘normal year*’ rainfall as the basic reference scenario.
Enhanced	10	916.3	Adding one ‘extreme year#’ rainfall

			following every two ‘normal year’ rainfall
Intensified	10	1026	Multiply normal rainfall by 1.5

*The rainfall in the year of 2016 is used to represent a ‘normal year’ rainfall.

The rainfall in the year of 2013 is used to represent an ‘extreme year’ rainfall.

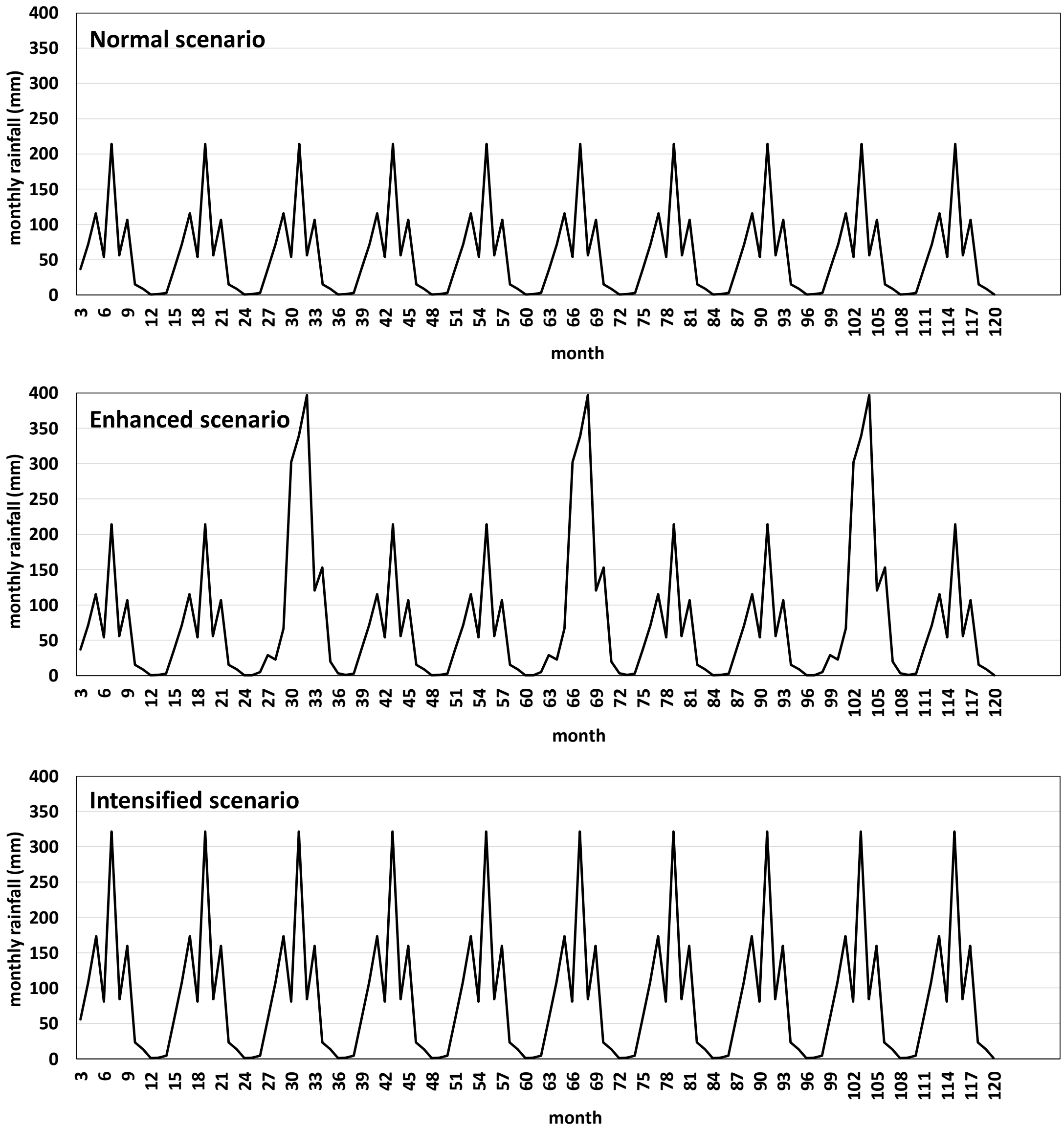

Fig. 7. Three hypothetical rainfall scenarios (normal, enhanced and intensified).

4. Results and discussion

4.1. Modeling the 2013 events

Discharge and sediment yields at the outlet of the watershed were simulated on daily time steps. Figure 8 shows two abrupt rises in the sediment yield at the outlet of the catchment, which are associated with the two severe rainfall events that occurred in July and August 2013. The DEM was updated at the end of each simulated year to update the sediment yields and determine the local terrain changes. The spatial patterns of erosion and deposition were generated by comparing the updated DEM with the initial DEM. As shown from the modeling results in Fig. 9, the landform changes in the study basin were concentrated mainly in the river channel. The downstream channel experienced more from the impacts of flooding than the upstream channel. Most of the drainage system in the basin experienced erosion because of extreme rainfall events, which generated substantial deposition downstream in the main channel. The loose materials accumulated on hillslopes and in valleys were transported into the river channel by debris flows, which resulted in the aggradation of riverbeds.

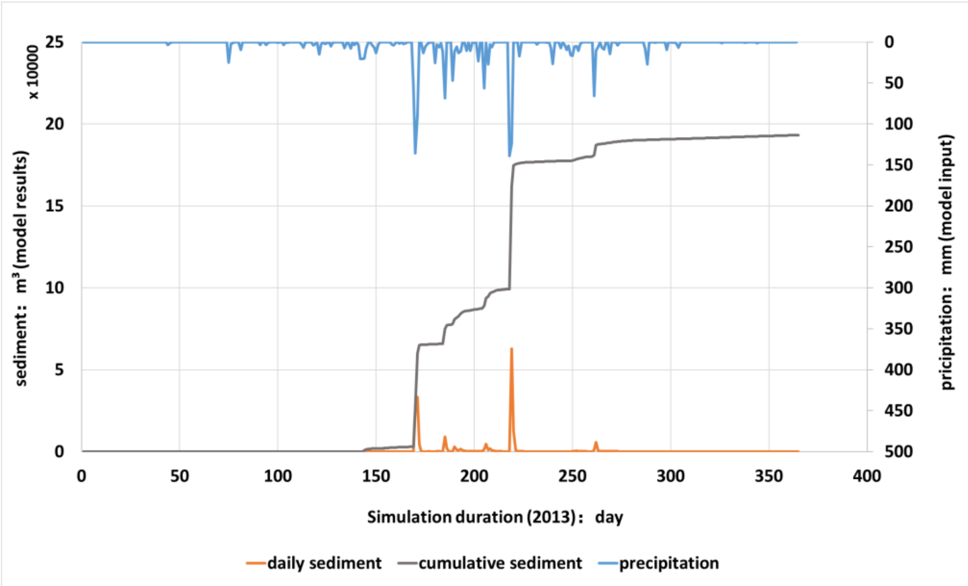

Fig. 8. Precipitation and sediment yield in 2013 from modeling results.

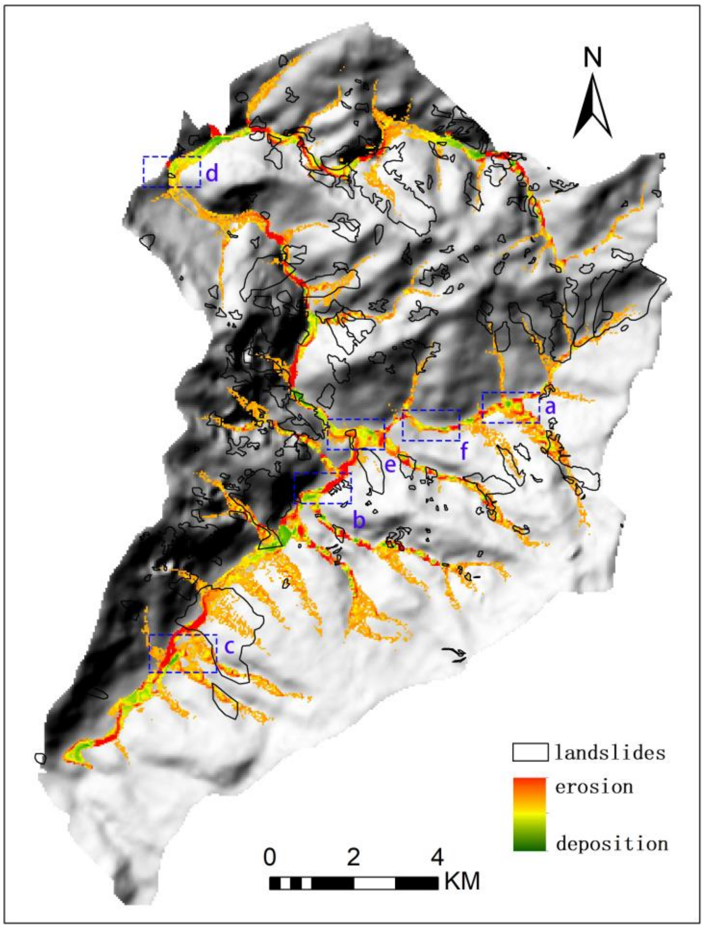

Fig. 9. Spatial distribution of erosion and deposition from modeling results.

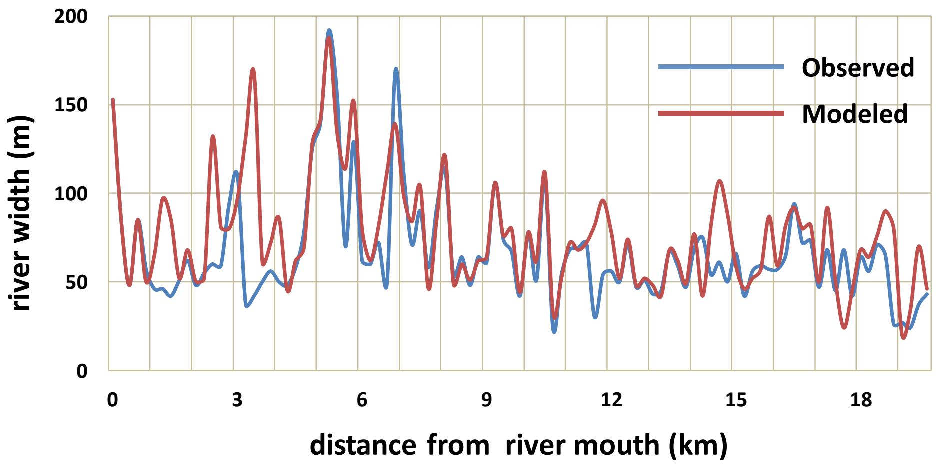

Fig. 10. Comparison between modeled and observed channel widths after 2013 flooding.

By extracting the impacted area (due to either erosion or deposition >0.5 m) from the modeling results, we conducted a quantitative model validation by comparing the modeled 'impacted' area with the observed channel after the 2013 flooding from satellite images combined with field reconnaissance. As shown in Fig. 10, the modeled results are generally in agreement with the observed impacted width of river channels. Nevertheless, the lower reach still displays a relatively larger difference. The observed impacted river channel area after the 2013 flooding is 132.7 ha, while the channel impacted area from the modeling results (erosion and deposition) is 152.8 ha, indicating a good overall performance of the CAESAR-Lisflood when simulating the 2013 flooding event.

Based on high-resolution satellite images (SPOT6 in 2012 and IKONOS in 2013 as listed in Table1) and field reconnaissance in the study area, we used six sites (indicated on Fig. 9) as reference locations to identify the typical fluvial processes to further check the reliability of the modeled results (Fig. 11). By comparing the satellite images between 2012 and 2013, we can see that the river channel experienced significant change after the rainfall-induced floods during the summer of 2013. Many parts of the riverbeds became wider and filled with debris. Some parts of the riverbeds experienced severe erosion and affected houses and dikes nearby. For example, the river channel shown on the right in Fig. 11a had obvious debris accumulation and wider riverbeds. The modeling results show that the right part of the river had a large amount of deposition (denoted by blue) and agrees with the field observations. The river channel shown in Fig. 11b experienced erosion on the left bank and deposition on the right bank. The houses at the left bank were completely washed away during the 2013 flooding. The modeling results show that the locations of those houses (denoted by purple) experienced severe erosion (denoted by red), which could lead to the collapse of those houses. Figures 11c, d and e show that similar fluvial processes occurred during the 2013 flooding, and in general, the modeling results agreed well with the observations from both satellite images and field reconnaissance. In Fig. 11f, the riverside road was also destroyed by flood scouring. The road was in a low location beside the riverbed at the bottom of two steep valleys, and two large landslides moved down into the channel; this resulted in constant scouring of the opposite bank, which eroded the road. Furthermore, loose material derived from the landslides filled the river channel with sediment. The riverbed aggraded in most parts of the downstream channel from sediments deposited during the flash flooding.

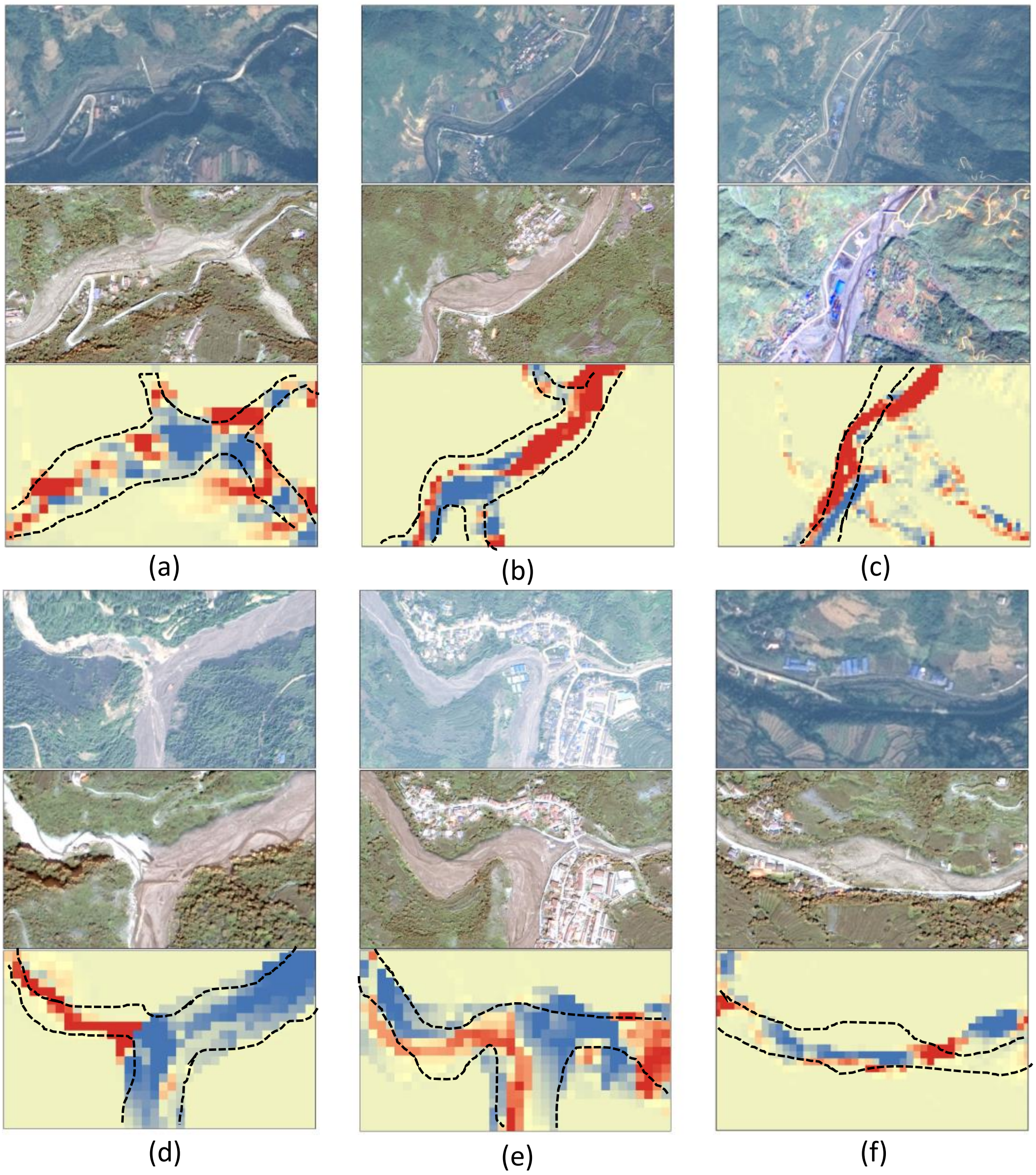

Note: Each site has 3 pictures. The picture of the first row shows image of 2012 before the flooding; second row shows image of 2013 after flooding; third row shows deposition (blue) and erosion (red) from the modeling results. The dash lines denote the observed impacted area along river channel from images and field reconnaissance.

Fig. 11. Typical sites of erosion and deposition in the river channel.

To further validate the model at a vertical scale, we chose four sites (location #1, #2, #3, #4 as shown in Fig. 12a) to measure the height of the deposition during the field work in 2012 and 2013. We estimated the elevation changes in the river channel by measuring the reference objects (buildings and bridges), as shown in Fig. 12b, before and after the

2013 flooding event and used the measured difference as an approximation of the change in riverbed elevation. The elevation changes of modeling results (Fig. 12c) were extracted by subtracting the initial DEM from the modelled DEM after the 2013 flooding event. We generated the cross sections from the modeling results to calculate the depositional thickness of the channel. Figure 13 summarizes the comparison between changes measured in the field and the modelled elevations.

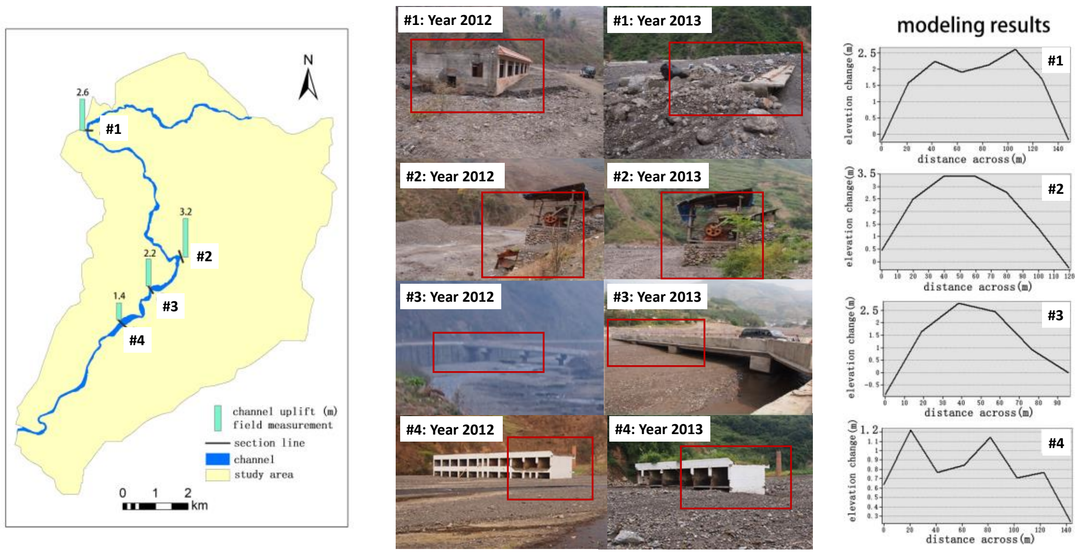

(a) Study area and locations (#1, #2b, #3, #4) for field measurement

(b) Photos of measurement locations in 2012 (before flooding) and in 2013 (after flooding)

(c) Modeled elevation changes at locations #1, #2, #3 and #4.

Fig. 12. Deposition of four locations along the river channel from both field measurement and modeling results after the 2013 flooding event.

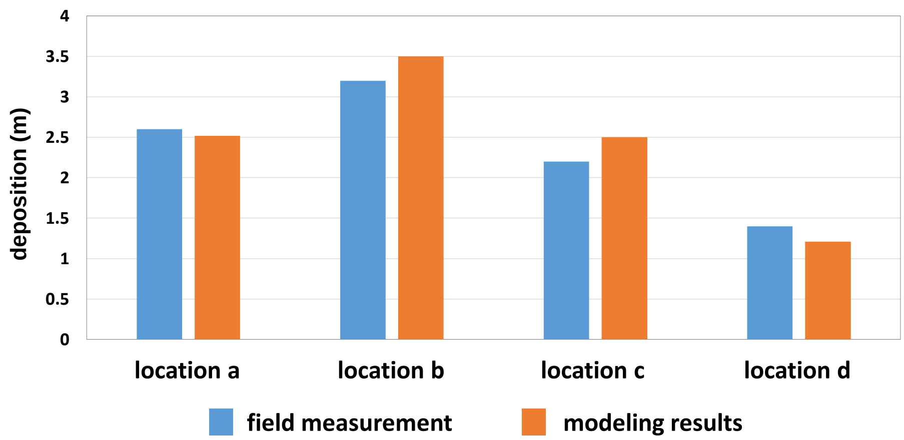

Fig. 13. Comparison between field measurements and model results of typical sites in Fig. 12.

Field surveys carried out in September 2013 indicated that the infrastructure affected by floods along the river were mainly concentrated in four locations (Yang et al., 2015). Along the sides of the channel, through field observation and measurement, Jiankang (location #2 in Fig. 12) recorded the highest amount of deposition (average >3.2 m) because it was located at the junction of two main rivers in the catchment. In addition, the other three sites aggraded approximately 1-3 m. Comparing these measurement values to the model results at these four sites (Fig. 13) shows that the modeled thicknesses of deposition in the channel are very close to the values measured in the field, indicating that the modeled results were well adapted to replicate the actual situation that occurred in 2013.

4.2. Modeling future scenarios

The results of modeling future scenarios (Fig. 14) show that the catchment sediment yield displays a temporal pattern in response to the rainfall variability. Sediment yield is usually an episodic process rather than a smooth and continuous one. The enhanced rainfall scenario produced a greater sediment yield than the normal rainfall scenario in response to the extreme rainfall event during 2013. Moreover, the intensified rainfall caused the greatest sediment yield at the outlet of the catchment, indicating that the rainfall is the dominant factor in the production and movement of sediments, thus causing the landscape to evolve in specific areas. There will likely be a large amount of uncertainty in the fluvial evolution processes in post-earthquake areas in response to the variability in rainfall.

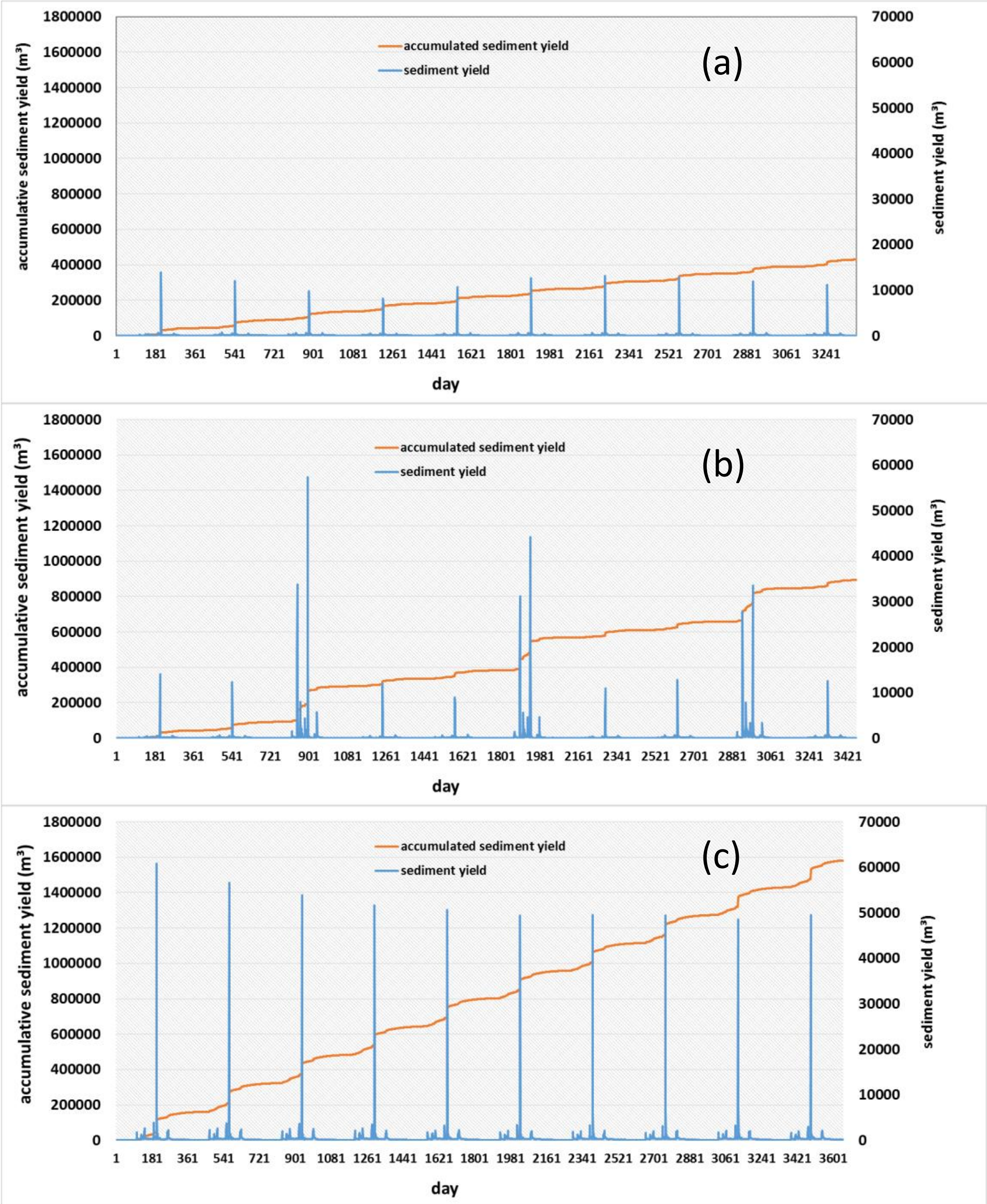

Fig. 14. Sediment yield from normal (a), enhanced (b) and intensified (c) rainfall scenarios.

Figure 15 shows spatial patterns of the erosion and deposition for the three future rainfall scenarios. For all scenarios, the erosion is more severe in the upstream areas of the basin, especially in river valleys. The deposition mainly appears in relatively flat and broad channels, particularly the downstream areas. The severity of erosion in the upstream river channels and mountain gullies and the amount of deposition in the downstream channels show a significant increase under enhanced and intensified rainfall scenarios. The maximum amount of deposition for the normal scenario is about 3.68 m, which is almost half of that for the enhanced and intensified scenarios. The maximum depth of deposition reached 7.63 m for the enhanced scenario and 7.71 m for the intensified scenario. The maximum depth of erosion for the three different scenarios varies between 6.83 m and 8.11 m.

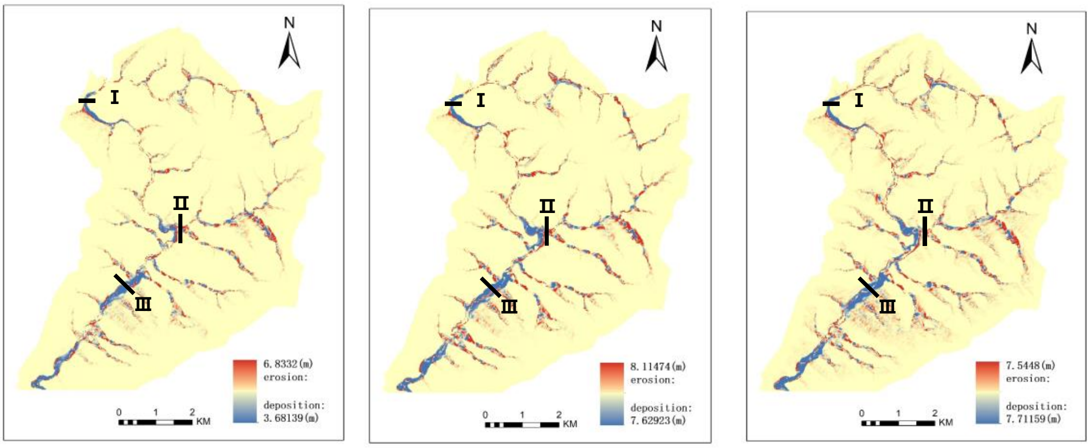

Fig. 15. Spatial patterns of erosion and deposition in study basin for the normal (left), enhanced (middle) and intensified (right) rainfall scenarios.

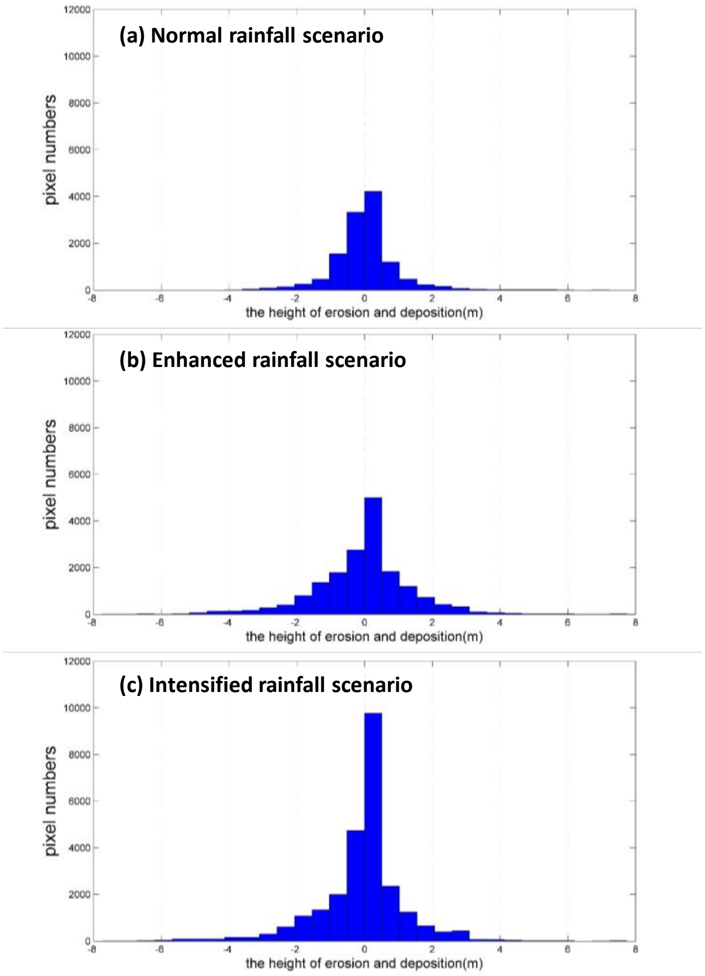

Fig. 16. Pixel distribution of Erosion (positive) and deposition (negative) for the different rainfall scenarios.

Table 4 Sediment production, sediment yield, and deposition for the different scenarios.

Scenarios	Total sediment production (10^6 m³)	Sediment yield at basin outlet (10^6 m³)	Sediment delivery ratio	Deposition in main channel (10^6 m³)	Deposition in study area (10^6 m³)	Proportion
	V1	V2	V2/V1	V3	V4	V3/V4
Normal	3.61	0.83	23.0%	0.85	1.56	54.5%
Enhanced	8.18	1.45	17.7%	2.05	3.67	55.9%
Intensified	10.14	1.58	15.6%	2.50	4.59	54.5%

Figure 16 shows histograms of pixels with erosion (negative values) or deposition (positive values) for each scenario in the basin. The histograms for each scenario are approximately normally distributed and symmetric. Significantly, more pixels would be affected in the enhanced and intensified scenarios than those in the normal scenario.

The modeling results (Table 4) show that the total sediment production for the entire basin rises from 3.61 million m^3 under the normal scenario to 8.18 and 10.14 million m^3 under the enhanced and intensified scenario, respectively. The sediment production increases nonlinearly from a normal scenario to the enhanced and intensified scenarios. The rainfall increased by 50% from the normal scenario to the intensified scenario, while the total sediment production in the basin increased by 180%. Although the sediment yield from the basin outlet also increased from 0.83 million m^3 under the normal scenario to 1.58 million m^3 under the intensified scenario, the growth rate of the sediment yield from the outlet is far below that of the sediment production within the entire basin. The sediment delivery ratio (Table 4) was lower for the enhanced and intensified rainfall scenarios. The modeling results show that the amount of material transported out of the basin constitutes only a relatively small portion of the total sediment produced in the whole basin, implying that there is significant sediment storage within the basin, and that this storage increases with an increase in the frequency and intensity of extreme rainfall events. This sediment is mostly stored in the valleys and low flat areas, and then transported to the main channel triggered by the major rainfall events. The proportion of sediment deposited in the main channel to the total deposition volume in the study area is over 50% for all three rainfall scenarios.

We further identified the river channel changes and spatial patterns of erosion and deposition from the three selected sites along the channel (Fig. 17). The modeling results show that the channel appeared to have a different degree of aggradation upstream (Location I) compared to downstream (Location III). The intensified scenario produced the largest amount of aggradation (up to 5 m), while the normal scenario produced the least amount of change in the cross section. These locations with significantly increased channel deposition could decrease channel conveyance capacity and lead to a higher risk of flash flooding, which would threaten the residential houses near the riverbanks. At Location II, the river channel was eroded, especially during the enhanced scenario, and under this scenario, the riverbed would be incised as much as 5 m.

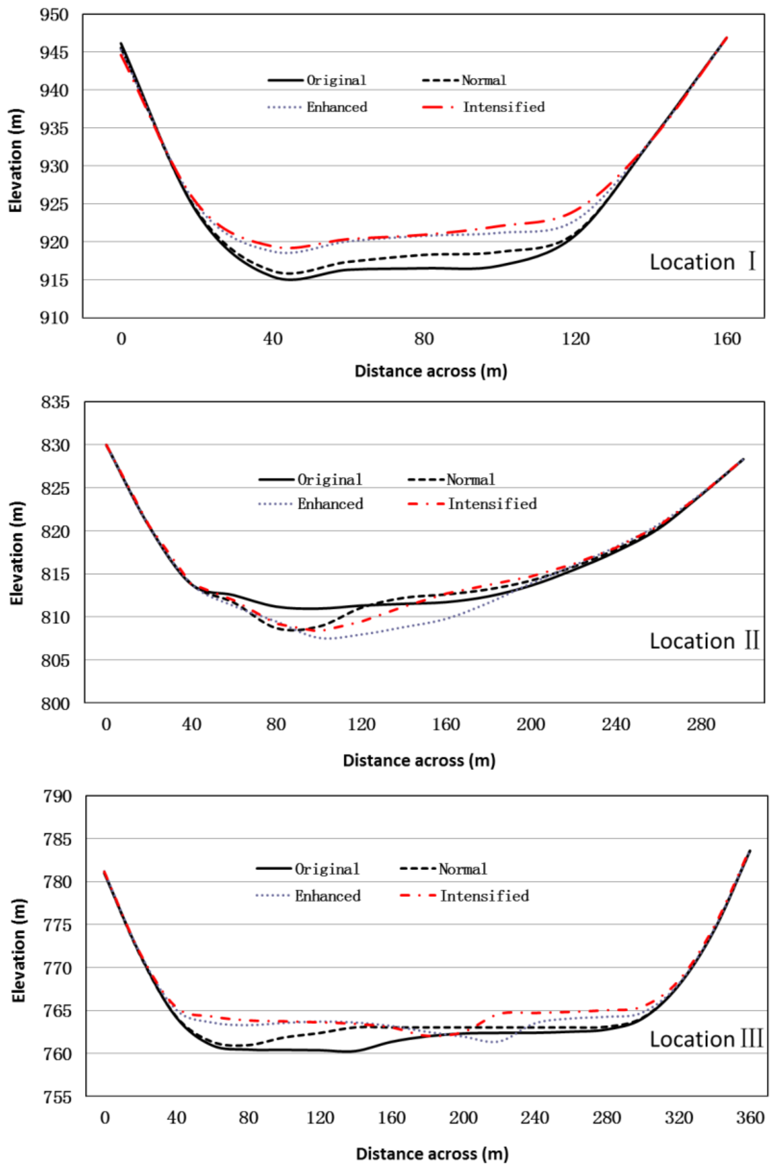

Fig. 17. Cross-sectional change at three typical sites along the river channel from upstream (Location I) to downstream (Location III).

The landslips and mass movements in this basin are still active after the major earthquake, and the uncertainty of future rainfall regimes may exaggerate the mass movement and deposition of mountainous loose materials in the riverbeds, as well as their linkage with flooding in the context of regional climate change. Hancock et al. (2016) suggested that the highest sediment loads would occur for the first 10-yr post-construction in disturbed areas, which is similar to the results found in previous assessments (Hancock et al., 2015). The threat of subsequent hazards occurring in mountainous regions after a major earthquake could be sustained for a very long time, from years to decades (Huang and Li, 2014). The large amount of loose material and debris induced by an earthquake can be further triggered to move downward during severe rainfall events. In this study, we focused mainly on the landform evolution during the decade following the earthquake, particularly the fluvial processes during this time that are most likely to be affected by the variability in rainfall. This 10-yr period is also an important time for the assessment and management of post-earthquake reconstruction.

5. Conclusions

CAESAR-Lisflood was initially developed to examine natural catchment hydrology and geomorphology, and it has become a common tool for simulating geomorphic behaviors such as erosion and depositional changes in river catchments over a wide range of temporal and spatial scales. This is the first time that a landscape evolution model has been employed to model landform evolution and sediment migration in a post-earthquake area. In particular, CAESAR-Lisflood is well adapted to simulate the fluvial processes of landscape evolution in this study. The modeling results after parameter adjustment and verification show that CAESAR-Lisflood could simulate the local landform changes well, especially the river channel areas driven by extreme meteorological disasters such as floods. The model can replicate both spatial and vertical heterogeneity of the sediment movement that occurred in the past as the result of an earthquake.

Modeling results under normal, enhanced and extreme rainfall scenarios showed that the intensity and frequency of extreme rainfall could produce dramatic impacts on landscape changes, especially fluvial processes. In the process of landscape evolution, rainfall dominates discharge and flooding events in the watershed, which affects the sediment transportation process and the landscape evolution process. Moreover, the modeled sediment yield increased nonlinearly with an increase in the frequency and intensity of extreme rainfall events (i.e., from a normal scenario to the enhanced and intensified scenarios). Both spatial and vertical patterns of landforms changed significantly, especially in areas near the river channel and mountain gullies during all three scenarios.

The large number of landslides triggered by the Wenchuan earthquake produced a significant impact on sediment production in the entire study basin. During severe rainfall events, sediment from landslides were transported to lower reaches, especially the main channel. Meanwhile, the movement and deposition of sediment in earthquake-stricken areas caused aggradation of riverbeds, which make the study area extremely susceptible to flash floods that creates further risks to the newly rebuilt houses that are close to the river.

It is crucial to clarify sediment yield and landform changes after major earthquakes in mountainous regions. This research modeled the sediment movement and channel change response to rainfall variability. To mitigate the risks caused by fluvial processes under specific rainfall scenarios, effective engineering and ecological measures should be taken in accordance with modeled results.

Acknowledgments

This research was supported by the National Natural Science Foundation of China under grants 41671503 and 41621061. This research was also sponsored by CBDM Asia Programme (Phase II), International Center for Collaborative Research on Disaster Risk Reduction (ICCR-DRR).

References

Bates, P.D., Horritt, M.S., Fewtrell, T.J., 2010. A simple inertial formulation of the shallow water equations for efficient two-dimensional flood inundation modelling. Journal of Hydrology 387(1), 33-45.

Beven, K., 1997. TOPMODEL: a critique. Hydrological Processes 11(9), 1069-1085.

Chang, K.J., Taboada, A., Chan, Y.C., Dominguez, S., 2006. Post-seismic surface processes in the Jiufengershan landslide area, 1999 Chi-Chi earthquake epicentral zone, Taiwan. Engineering Geology 86(2–3), 102-117.

Chen, J.-g., Chen, X.-q., Wang, Y.-h., Zhong, W., 2014. Types and Causes of Debris Flow Damage to Drainage Channels in the Wenchuan Earthquake Area. Journal of Mountain Science 11(6), 1406-1419.

Chen, R.F., Chang, K.J., Angelier, J., Chan, Y.C., Deffontaines, B., Lee, C.T., Lin, M.L., 2006. Topographical changes revealed by high-resolution airborne LiDAR data: the 1999 Tsaoling landslide induced by the Chi–Chi earthquake. Engineering Geology 88(3), 160-172.

Chen, X., Zhiguang, L.I., Cui, P., Liu, X., 2009. Estimation of Soil Erosion Caused by the 5•12 Wenchuan earthquake. Journal of Mountain Science 27(1), 122-127.

Coulthard, T.J., Hicks, D.M., Wiel, M.J.V.D., 2007. Cellular modelling of river catchments and reaches: Advantages, limitations and prospects. Geomorphology 90(3), 192-207.

Coulthard, T.J., Macklin, M.G., Kirkby, M.J., 2002. A cellular model of Holocene upland river basin and alluvial fan evolution. Earth Surface Processes & Landforms 27(3), 269-288.

Coulthard, T.J., Neal, J.C., Bates, P.D., Ramirez, J., Almeida, G.A.M.D., Hancock, G.R., 2013. Integrating the LISFLOOD–FP 2D hydrodynamic model with the CAESAR model: implications for modelling landscape evolution. Earth Surface Processes & Landforms 38(15), 1897-1906.

Coulthard, T.J., Wiel, M.J.V.D., 2013. 9.34 Numerical Modeling in Fluvial Geomorphology. Treatise on Geomorphology, 694-710.

Coulthard, T.J., Wiel, M.J.V.D., 2017. Modelling long term basin scale sediment connectivity, driven by spatial land use changes. Geomorphology 277, 265-281.

Cui, P., Zhu, Y.Y., Han, Y.S., Chen, X.Q., Zhuang, J.Q., 2009. The 12 May Wenchuan earthquake-induced landslide lakes: distribution and preliminary risk evaluation. Landslides 6(3), 209-223.

Hancock, G., R., Coulthard, T., J., Martinez, Kalma, J.D., 2011. An evaluation of landscape evolution models to simulate decadal and centennial scale soil erosion in grassland catchments. Journal of Hydrology 398(3), 171-183.

Hancock, G.R., Lowry, J.B.C., Coulthard, T.J., 2015. Catchment reconstruction — erosional stability at millennial time scales using landscape evolution models. Geomorphology 231, 15-27.

Hancock, G.R., Verdon-Kidd, D., Lowry, J.B.C., 2016. Sediment output from a post-mining catchment - centennial impacts using stochastically generated rainfall. Journal of Hydrology 544.

Huang, R., Li, W., 2014. Post-earthquake landsliding and long-term impacts in the Wenchuan earthquake area, China. Engineering Geology 182, 111-120.

Korup, O., 2009. Linking landslides, hillslope erosion, and landscape evolution. Earth Surface Processes & Landforms 34(9), 1315-1317.

Korup, O., Densmore, A.L., Schlunegger, F., Glade, T., Crozier, M.J., 2010. The role of landslides in mountain range evolution. Geomorphology 120(1), 77-90.

Li, C., Wang, M., Liu, K., Xie, J., 2018. Topographic changes and their driving factors after 2008 Wenchuan earthquake. Geomorphology 311, 27-36

Qi, L., Wang, Z.Y., Wang, X., 2012. Erosion and sediment budget of the 2008 Wenchuan earthquake: a case study on Mianyuan River basin. Natural Science 4(8A), 640-647.

Tang, C., 2010. Activity Tendency Prediction of Rainfall Induced Landslides and Debris Flows in the Wenchuan earthquake areas. Journal of Mountain Science 28(3), 341-349.

Tang, C., Zhu, J., Qi, X., Ding, J., 2011. Landslides induced by the Wenchuan earthquake and the subsequent strong rainfall event: a case study in the Beichuan area of China. Engineering Geology 122(1), 22-33.

Wang, J., Jin, Z., Hilton, R.G., Zhang, F., Densmore, A.L., Li, G., West, A.J., 2015. Controls on fluvial evacuation of sediment from earthquake-triggered landslides. Geology 43(2), 115-118.

Wang, M., Yang, W., Shi, P., Xu, C., Liu, L., 2014. Diagnosis of vegetation recovery in mountainous regions after the Wenchuan earthquake. IEEE Journal of Selected Topics in Applied Earth Observations & Remote Sensing 7(7), 3029-3037.

Wiel, M.J.V.D., Coulthard, T.J., Macklin, M.G., Lewin, J., 2007. Embedding reach-scale fluvial dynamics within the CAESAR cellular automaton landscape evolution model. Geomorphology 90(3), 283-301.

Xu, Q., 2009. Studies of major types and characteristics of earthquake-induced geological disasters. Journal of Geological Hazards and Environment Preservation 20(2), 86-93.

Yang, W.T., Wang, M., Kerle, N., Westen, C.J., Liu, L.Y., Shi, P.J., 2015. Analysis of changes in post-seismic landslide distribution and its effect on building reconstruction. Natural Hazards & Earth System Science 15(4), 817-825.